University of Bath
Centre for Sustainable Chemical Technologies
Department of Chemistry

Computational Investigation of the Properties and Performance Bottlenecks of Selected Metal Sulfides for Use as Solar Absorber Materials

Suzanne K. Wallace

May 11, 2016

Abstract

CZTS as a promising earth-abundant non-toxic solar absorber material for thin-film photovoltaic devices, theoretical conversion efficiency of 28 % but major bottleneck of low open circuit voltage (V_{OC}) relative to the band gap of the material. Highlight importance of interpreting PL spectra for PV materials?

Candidate photoferroelectric materials from screening process and properties for PV that we predict.

Address why metal sulphides?

Acknowledgements

I would like to express (whatever feelings I have) to:

- My supervisor
- My second supervisor
- Other researchers
- My family and friends

Contents

List of Tables

List of Figures

Chapter 1

Introduction

1.1 The Case for New Solar Absorber Materials for Photovoltaic Devices

1.1.1 Terawatt-Scale Energy Production from Renewable Resources

It is now widely accepted that the world is heading towards a major energy crisis, where there will come a point that the current major sources of energy (namely fossil fuels) will be unable to meet increasing global demand for energy as they are not a limitless supply. Furthermore, there is the ever present worry of climate change linked to increased carbon dioxide emissions from the burning of fossil fuels. Renewable, low-carbon alternative energy sources are therefore clearly desirable. From purely environmental considerations, it seems clear that fossil fuels should no longer be used and we should meet our energy needs solely from renewable, low-carbon energy resources such as solar power. However, it is not only environmental sustainability that must be considered, we must also consider the economical feasibility of solar power for large-scale projects. Germany is an example of a country making considerable efforts to increase the percentage of their energy supplied by solar power. On June 9 2014 Germany even generated over 50% of its electricity demand from solar for the first time [78]. Although on average the country is not able to produce such a large portion from solar power, with solar-generated power

providing approximately 7.5% of net electricity consumption in 2015 [79]. To facilitate the growth of the solar power capacity in Germany a number of schemes and financial incentives to encourage investment were introduced, such as feed-in tariffs (FiTs). The German government first introduced FiTs in their Grid Feed-In Law (the Stromeinspeisegesetz), which came into force in 1991 [46]. FiTs are intended to support new developments in renewable energy supply by providing investor certainty. They set the rate a utility company must pay for renewable generated energy and guarantee the provider of renewable energy a specific rate for a long period of time, typically fifteen to twenty years. As this cost is higher than fossil fuel based electricity, the higher price is then passed on to all customers of the utility company to spread out the higher costs so that buyers of renewable energy do not pay higher prices. In Germany, this has resulted in an increase of 6% on the average electricity bill for users in a specific region [52]. The social implications of such a cost increase must also be considered in assessing the viability of a particular power source.

Solar power, however, is still a realistic candidate for replacing fossil fuels as a major supply of global energy. It is by far the largest source of energy available to us, as illustrated in figure 1.1, and it is also the most widely geographically distributed [35]. The Sun supplies 3×10^{24} J of energy to the Earth each year, which is 10^4 times more than mankind's current annual energy consumption. In theory, this would require only 0.1% of the Earth's surface to be covered in solar cells with a conversion efficiency of just 10% to satisfy our current energy needs [27]. Recent years have seen a rapid increase in the installed solar generation capacity, with the global grid-connected PV capacity growing from 1.3 GW in 2000 to 139 GW in 2014 [3], with approximately a doubling in the cumulative installed capacity every two years [38]. Additionally, creative business models have spurred investment in residential solar systems [53]. Great improvements in technology, price and performance have helped to facilitate this growth, but solar energy still only provides a minor fraction of the world's energy. In 2013 solar power only provided 0.87% of the worlds electricity [60]. Further advances are required to enable a dramatic increase in the contribution from solar power at socially acceptable costs [53]. Ultimately, solar power-generation technologies must become cost-competitive with conventional fossil-fuel based power sources.

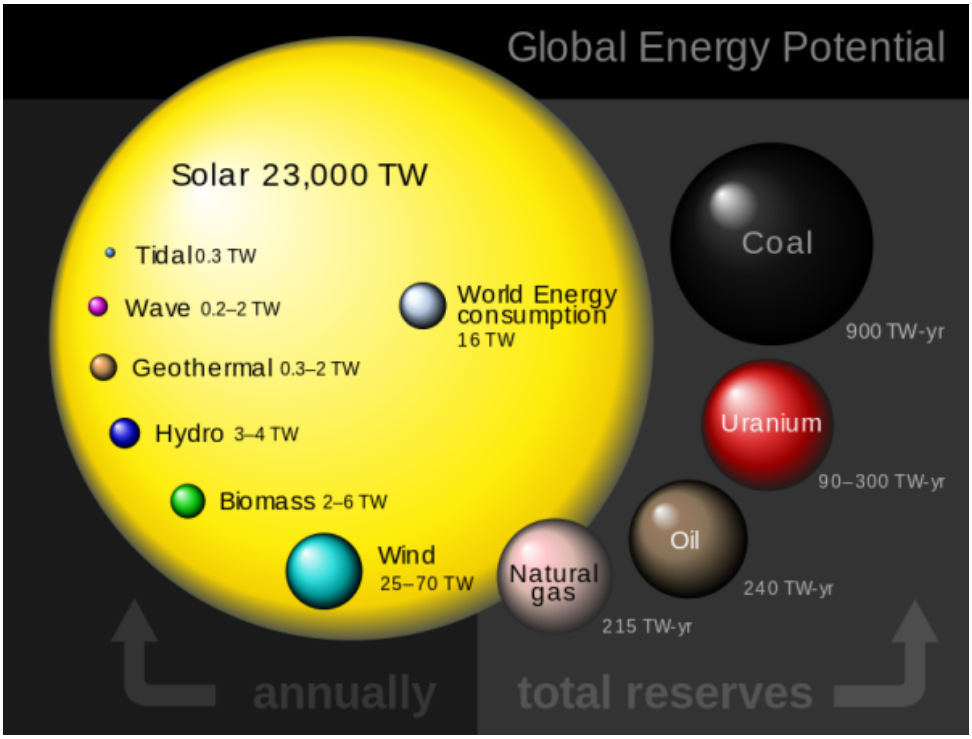

Figure 1.1: Illustration of power available annually from various renewable energy resources, annual world energy consumption and total reserves of various non-renewable energy resources. Figure take from 76.

Levelized cost of energy, or electricity, (LCOE) is a common way to assess how cost competitive renewable energy sources are with their non-renewable counterparts. LCOE allows for the measurement of the performance of different power generating technologies, which may have unequal lifetimes and differing capacities. It is calculated by summing all costs incurred during the lifetime of the technology and dividing this value by the units of energy produced during the lifetime, with units of energy expressed as dollars per kilowatt hour ($/kWhr) [48]. This measure is also used as the key selling point for a number of commercial solar cell manufacturers such as First Solar Inc., who market their product as being able to generate electricity at an average of $0.63 per Watt as stated in their 2013 Annual Report [34]. Using the LCOE, comparisons of grid competitiveness for renewable energy sources can be made [48]. Figure 1.2 shows the LCOE of renewable energy technologies and conventional power plants at locations in Germany in 2013, enabling an assessment of the cost-competitiveness of PV power generation at this location, accounting for, for example, typical solar irradiation at the given locations [21]. As the figure shows, both small-scale and large-scale utility solar power are still not cost

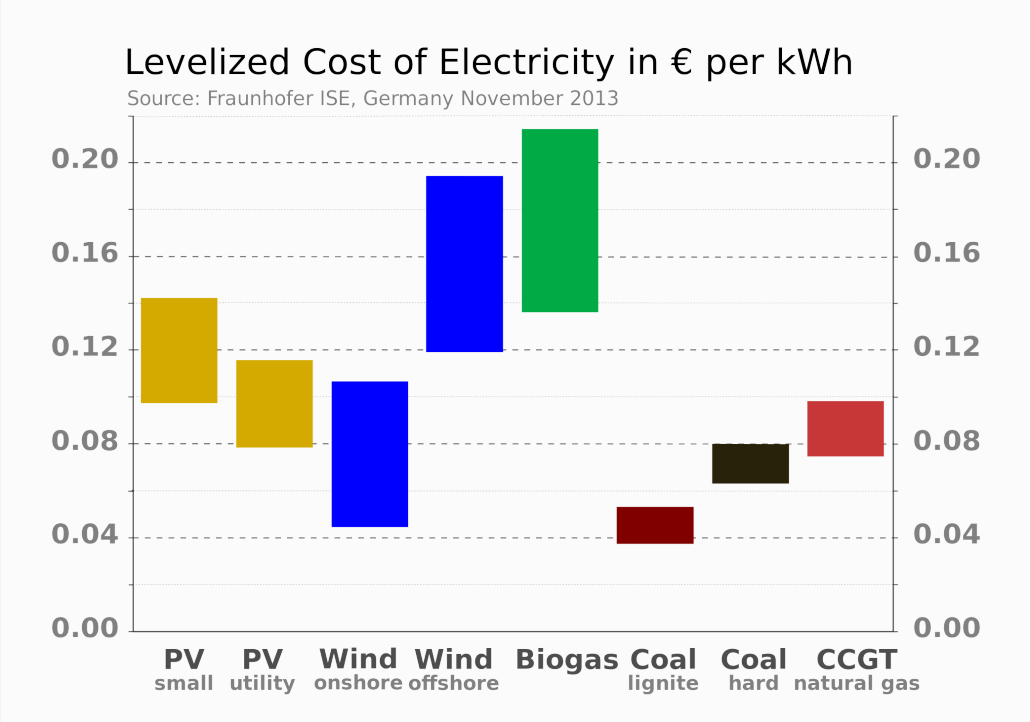

Figure 1.2: Levelized cost of electricity (LCOE) of renewable energy technologies and conventional power plants at locations in Germany in 2013. Specific investments are taken into account with a minimum and maximum value for each technology. Figure taken from reference 21.

competitive with the cheapest non-renewable resources.

1.1.2 Basic Operating Principles of a Solar Cell Device

test [10]

Voltage is generated in a solar cell by the photovoltaic effect. The terms 'solar cell' and 'photovoltaic (PV) cell' are therefore often used interchangeably. When semiconducting materials absorb photons of light with energies of at least their band gap, electrons are excited to higher energy states within the material to form an electron-hole pair, as shown in figure 1.3. The excited electron-hole pair would eventually recombine and relax back to the ground state of the material with the emission of a photon of an energy equal to the energy of the electronic transition that has just occurred. However in a PV device, there is a built-in asymmetry that leads excited charge-carriers away before they can recombine back to the ground state. The extra

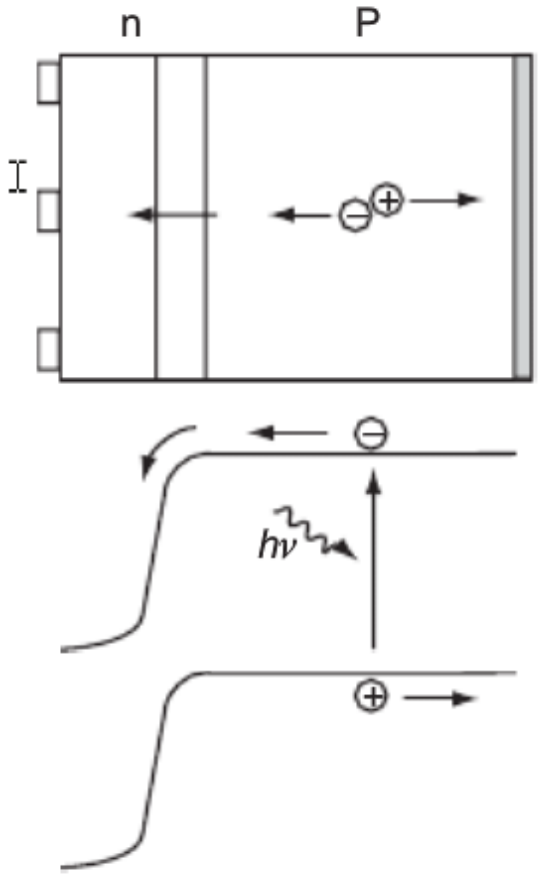

Figure 1.3: Schematic of a typical crystalline silicon solar cell device (top), where the majority of the cell consists of a thick p-type base in which most of the light is absorbed. After light absorption, the minority carriers (electrons) diffuse to the junction where they are swept across by the strong built-in electric field. The electrical power is collected by metal contacts to the front and back of the cell. Excitation of an electron-hole pair across the band gap of the p-type material (bottom). Figure taken from reference 49.

energy of the excited electron generates a potential difference that drives electrons through a load in the external circuit to do electrical work. In the conventional PV effect, as electrons are excited across the band gap of a semiconductor, the band gap of the material sets the upper limit for the maximum voltage that can be generated. In early PV devices, the asymmetric junction was a Schottky barrier between a metal and a semiconductor but now more effective p-n junctions are used, which are formed by joining together p-type and n-type semiconductors [50].

When a cell consisting of a p-n junction is illuminated, a voltage develops across the terminals, i.e. between the p-type and n-type semiconductors. When the terminals of the solar cell are

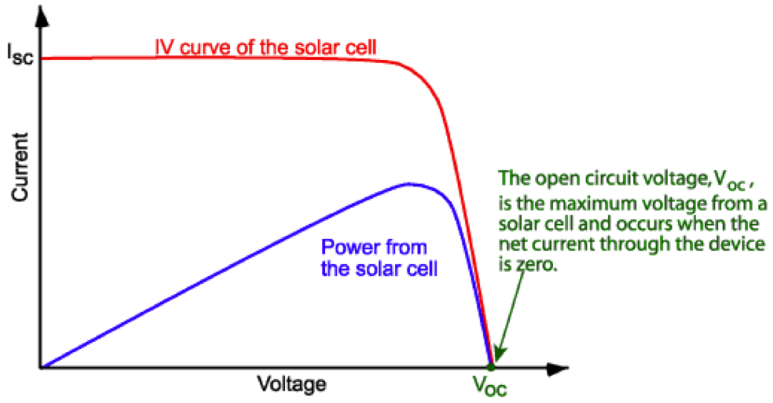

Figure 1.4: The current-voltage (I-V) curve of a solar cell showing the open circuit voltage (V_{OC}). Figure taken from reference 30.

disconnected from any external circuit, or there is an infinite load resistance, this voltage is at a maximum and is called the open circuit voltage (V_{OC}) and no current is drawn from the solar cell. Conversely, if the terminals of the solar cell are connected together then there is no voltage as all of the electromotive force is used to extract charge-carriers. The maximum possible current is drawn, which is called the short circuit current (I_{SC}). For a solar cell to generate power, there must be both voltage and current generated, therefore when the cell is operating at either V_{OC} or I_{SC} the power output is zero. To generate power, a finite load resistance is added to the circuit so that some current is drawn from the solar cell and a voltage develops across the cell that is between 0 and V_{OC} [50]. There is a maximum operation point for the power output (P_{MP}) of a solar cell in terms of I and V, as shown in figure 1.4. This can be defined in terms of V_{OC} and I_{SC} when used in conjunction with the fill factor (FF), which is a number less than one that describes the squareness of the I-V curve [28] shown in figure 1.4 and is given by equation 1.1. The current and voltage are determined by the load and illumination so the load can be tuned such that maximum power output is achieved, but the value of V_{OC} places a limit on the power output of the cell [50].

$$P_{MP} = FFV_{OC}I_{SC} \tag{1.1}$$

$$\eta = \frac{P_{MP}}{P_{in}} = \frac{FFV_{OC}I_{SC}}{P_{in}} \tag{1.2}$$

The power conversion efficiency (PCE), η, of a solar cell is the ratio of power output from the solar cell to the power input from the Sun. This is shown in equation 1.2, where P_{MP} has been taken from equation 1.1. For an efficient solar cell, it is desirable to have a high I_{SC}, a high V_{OC} and a FF that is as close to 1 as possible [28].

Move discussion to section on candidate new materials CZTS solar cells are known to be hampered by low V_{OC} relative to the band gap of the material [68]. Whereas in ferroelectric PV materials, photovoltages orders of magnitude larger than the band gap have been measured (a phenomena referred to as the anomalous photovoltaic effect), but very low photocurrent output is a big challenge for these devices [87].

Add figure and description of basic PV device + show basic simplified band diagram (later compare to real band structure, e.g. of Si

A solar cell device consists of... (see Mirjana's thesis)

1.1.3 Key Properties & Experimental Measurements to Assess Materials for Use in Solar Cell Devices

- PL
- band gap
- absorption coefficient
- effective mass
- dielectric function (screening of defects): Why dielectric function is important - lower dielectric const in CZTS suggests electrostatic potential fluctuation is long ranged, material will be less 'defect tolerant' - Look for textbook source!

1.1.4 Current Commercial Solar Cell Technologies & Limitations

It was first observed in 1839 by Edmond Becquerel that sunlight could be used to generate electricity. Becquerel discovered that if silver chloride was placed in an acidic solution, connected to platinum electrodes and exposed to sunlight, an electric current flowed. However the effect was small and poorly understood before Albert Einstein's discovery of the photoelectric effect and explanation of the phenomena by the quantum nature of light in 1904 [70]. Even then, it was not until the development of semiconductor technology during the silicon revolution of the 1950's that solar cells were fabricated which were able to generate significant amounts of electricity. The first silicon solar cell was created in 1954 in the Bell Laboratories with cells achieving efficiencies of 6%. Originally solar cells were developed for terrestrial energy generation, such as the 108 solar cells used to supply energy to the Vanguard satellite in 1958 [70]. The first oil crisis in 1973 however highlighted the dependency of many economies on fossil fuels and the need to address the security of energy supply, in particular for Japan and West Germany which had few of their own resources. As a consequence, solar cell research was no longer limited to only high-cost crystalline silicon devices for terrestrial applications, but also into creating cheaper, commercial, thin-film solar cell technologies using absorber materials such as amorphous silicon, cadmium telluride and copper indium diselenide [45].

In spite of this, crystalline silicon is still the dominant solar cell technology with mono- and poly-crystalline silicon photovoltaic cells comprising up to 90% of all the solar cells produced in 2008 [63]. Silicon is the second most abundant element in the Earth's crust [25], making it a plausible material to use in large-scale solar power generation. Over 60 years of development have seen device efficiencies increase from 6% to 25% for the highest quality research devices and 15-18% for the more common industrial cells [63]. As can be seen from figure 1.7, the best performing silicon devices are now very close to achieving conversion efficiencies close to their theoretical limit, as predicted by the Shockley-Quiesser detailed balance limit [67]. More dramatic however is the fall in manufacturing costs which have halved since 2008 and are more than a hundred times lower than they were in 1977, as shown in figure 1.5. This development

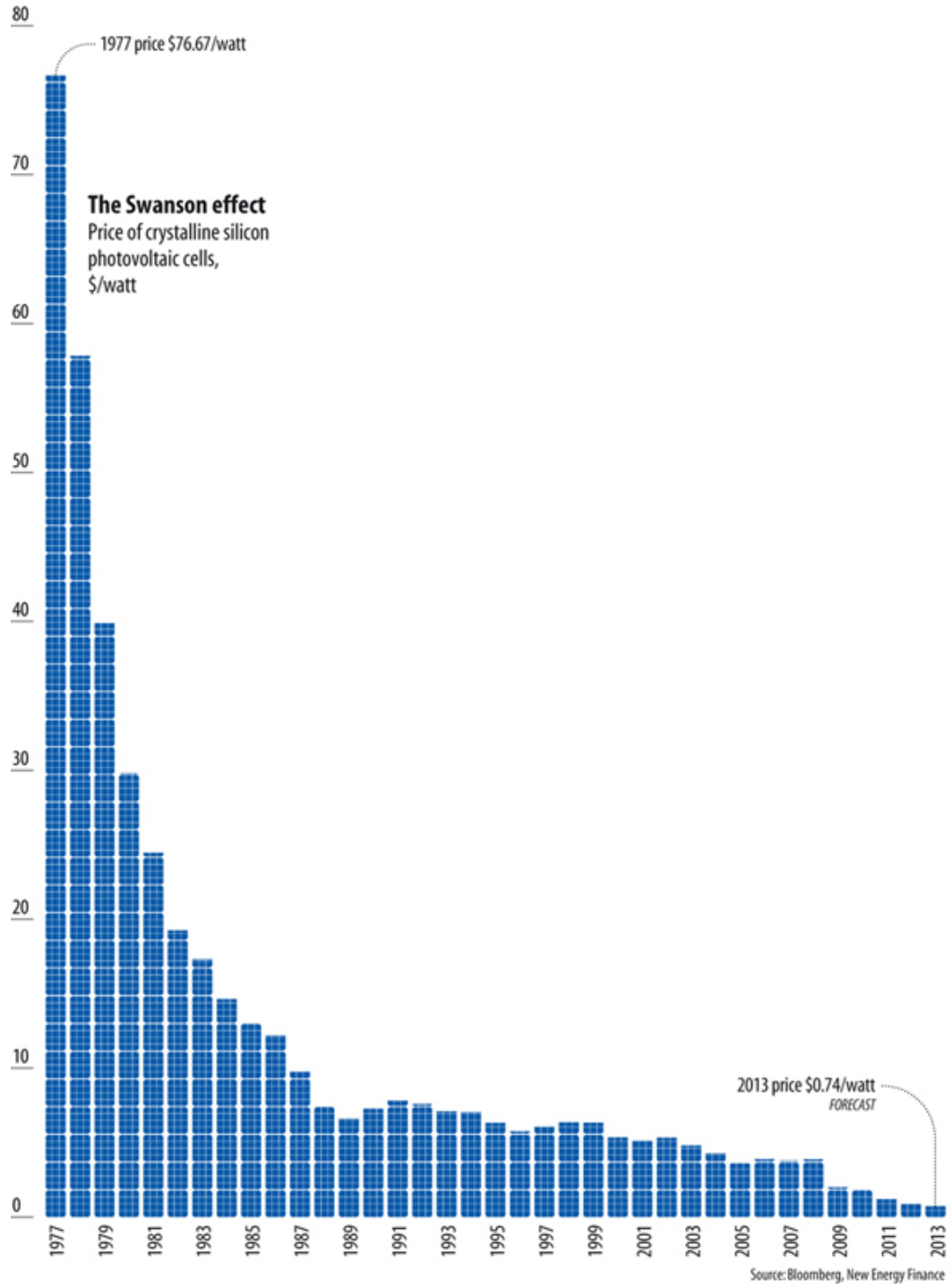

Figure 1.5:

was largely aided by progress in semiconductor technology driven by the silicon chip industry, with the solar industry benefiting from advances in silicon manufacturing processes and even making use of waste silicon produced that was not of a high enough grade for silicon chips [70]. Although the development of silicon-based technologies has clearly revolutionized the modern computer, the optical properties of silicon do not make it ideal for use as a solar absorber

material in a photovoltaic device and despite the dramatic reduction in manufacturing costs, the technology is still not able to be cost-competitive with fossil-fuel power generation, as was shown in figure 1.2.

The primary issue with silicon is that its band gap of 1.1 eV is indirect. The band structure of silicon is discussed in much more detail in section 2.3, but the key consequence of this property is that silicon is therefore not a very strong absorber of sunlight (compared to for instance newer, thin-film technologies which are discussed later), resulting in a low optical absorption coefficient compared to these newer technologies where both band gap and absorption coefficient were two of the key material properties for solar cells discussed in section 1.1.3. To absorb the same amount of sunlight with a silicon solar cell requires a thicker layer of the material than in thin-film technologies. Photovoltaic devices are very sensitive to defects and impurities. This point is discussed further in section 2.7, but the consequence for a thick layer of silicon is that very high quality, non-defective material is necessary to enable charge carrier collection before recombination occurs, which results in high manufacturing costs. The devices are made from flat sheets of crystalline or multicrystalline silicon called wafers that consist of very high quality silicon (99.999999% pure) [51]. The production processes of silicon wafers have been thoroughly optimised, but are still very energy-intensive, time-consuming and complex [29] and this is reflected by the position of this type of technology on the plot of efficiency versus cost shown in figure 1.6. Despite decades of development, commercialized silicon solar panels are still too expensive to compete with fossil-fuel based power sources [66].

The 'holy grail' of research into new materials for photovoltaic devices would be to find materials that are strong absorbers of sunlight that could also be produced cost-effectively from materials that are abundant enough for large-scale fabrication of the devices. Then it could be possible for solar energy generation to be economically viable on a large enough scale to replace fossil fuels to meet global energy needs. Such a drive has resulted in the development of what are considered three generations of solar energy technology. These are shown in figure 1.6, where highly efficient crystalline silicon devices with high associated manufacturing costs

are considered the first generation of solar cell technology. Thin-film solar cell devices are typically referred to as second-generation technology. These devices make use of materials that are much more optically thick than silicon (i.e. stronger absorbers of sunlight with higher optical absorption coefficients), which require less material to absorb the same amount of sunlight. It is then less important for the material to be of as high-quality as in crystalline silicon devices, which enables the use of low-cost and low-energy fabrication methods [29]. In the case of thin-film $CuInSe_2$ devices, it has even been found that the 'lower quality' poly-crystalline material has a higher performance than its single crystal counterpart [64, 62]. Theoretical studies of the electronic properties of the grain boundaries in $CuInSe_2$ have provided an explanation for this unusual observation based on beneficial band offsets at the grain boundaries [56, 57]. This effect is a special case for this particular material, but it embodies the general ideology of thin-film technology well - namely to produce materials able to convert sunlight into electricity as efficiently as possible with the simplest synthesis techniques possible. However typically the efficiencies of second-generation solar cells are less than that of the best performing first-generation devices. Examples of commercial thin-film technologies include CIGS ($Cu(In,Ga)(S,Se)_2$) and CdTe and figure 1.7 shows that the best performing Si devices have higher efficiencies, which are also much closer to their theoretical limit, than these second-generation, thin-film technologies. Third-generation PV technology aims to make use of the low cost fabrication techniques of the second-generation devices but use multiple energy threshold devices to overcome the Shockley-Quiesser limit for a single band gap solar cell, such as in tandem solar cells where semiconductor p-n junctions of increasing band gap are placed on top of each other in order to capture more of the solar spectrum. Typically the more complicated device architecture of third-generation devices result in higher fabrication costs. Research efforts are therefore largely focused on reducing the fabrication cost of multi-junction devices [81].

Current mainstream solar cell technologies, such as first-generation Si wafers and second-generation thin-film CdTe and CIGS solar cells, would not be able to provide solar electricity at the terawatt scale due to the scarcity of Te and In and the relatively long energy payback time for crystalline Si due to the cost and energy intensive fabrication of Si wafers [82]. In

order to significantly increase the contribution of solar power to global power consumption, it is therefore necessary to develop economically viable earth-abundant materials for sustainable PV electricity generation. Furthermore, there must be considerable technological breakthroughs that would enable low-cost manufacturing of highly efficient devices with enough of a cost benefit to outweigh the initial cost outlay in optimizing the manufacturing process of the whole device as has been done for silicon over the past 60 years. For this purpose, there is a drive for solar absorber materials with more optimal properties, such as a direct and sunlight matched band gap (as in thin-film technologies such as CdTe and CIGS), but also for materials that are composed of only earth-abundant components.

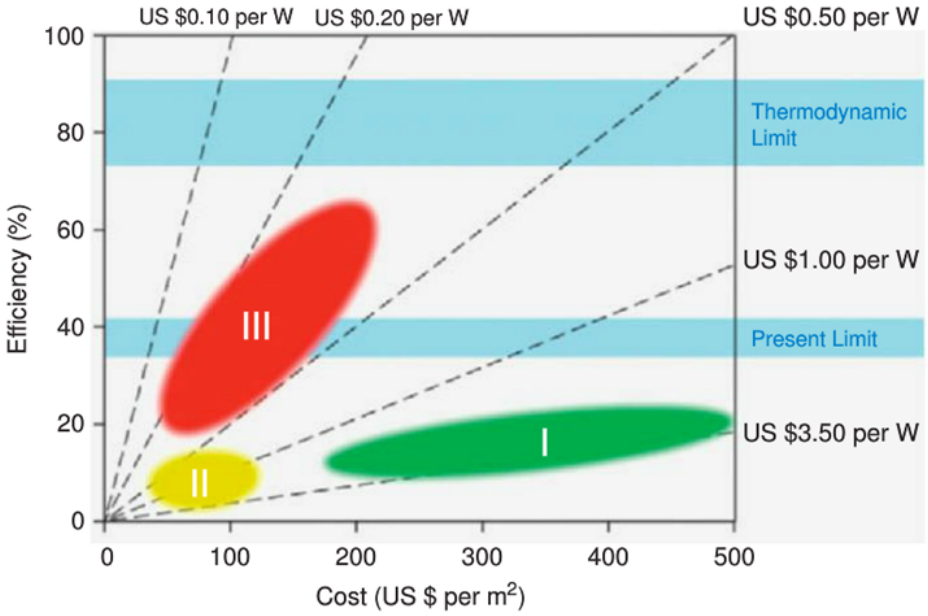

Figure 1.6: Efficiency and cost projections for first-, second- and third-generation photovoltaic technologies, which are comprised of silicon wafer, thin-film and advanced thin-film technology respectively. Figure taken from reference 24.

1.2 The Role of Computational Modelling in Material Design

See DFT in materials science paper

Prediction of properties and insight for experimentalists + material screening

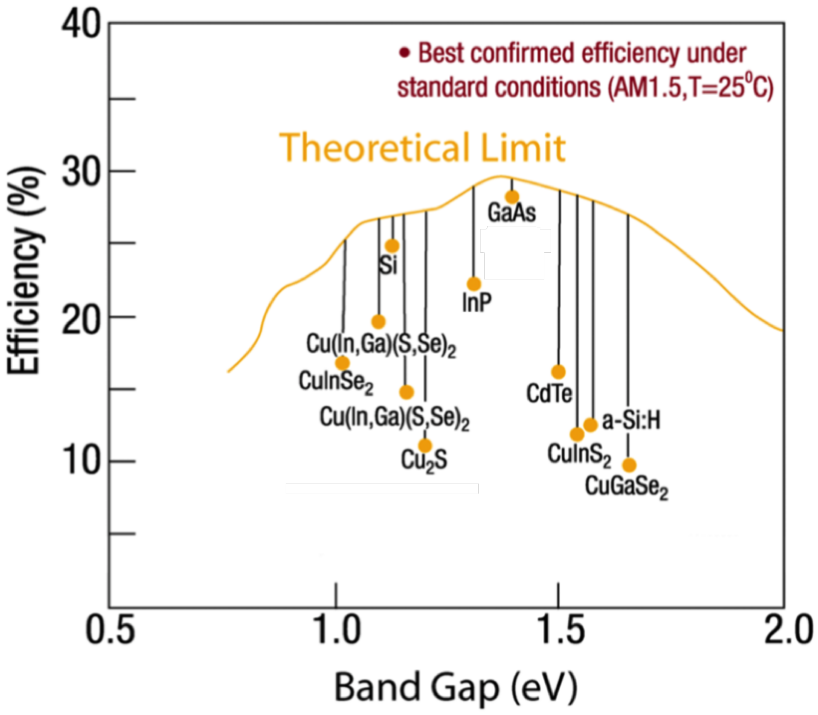

Figure 1.7: The Shockley-Queisser detailed balance limit of efficiency of p-n junction solar cells [67], showing the theoretical limit and current record efficiency for various photovoltaic technologies. Figure courtesy of LL Kazmerski (NREL).

There are two main contributions that computational simulations could make towards the technological breakthroughs needed for the development of photovoltaic devices for economically-viable, large-scale solar energy generation. Firstly by predicting properties and screening for certain desirable properties for a solar absorber material, such as an optimal band gap and high carrier mobility, materials simulations are able to aid in the discovery of new materials for use in photovoltaic devices. Secondly, material simulations are able to provide valuable insight to improve understanding of known photovoltaic materials to enable the synthesis of better performing devices. So far in this study we have aimed to make both of these contributions to the field. Firstly, we perform simulations to understand the performance bottlenecks in the candidate earth-abundant, non-toxic solar absorber material Cu_2ZnSnS_4(CZTS) and we also study the optical properties of three candidate photovoltaic materials which have so far received little attention as solar materials but could be another possible route for high-performance photovoltaic devices for cost-effective solar energy generation.

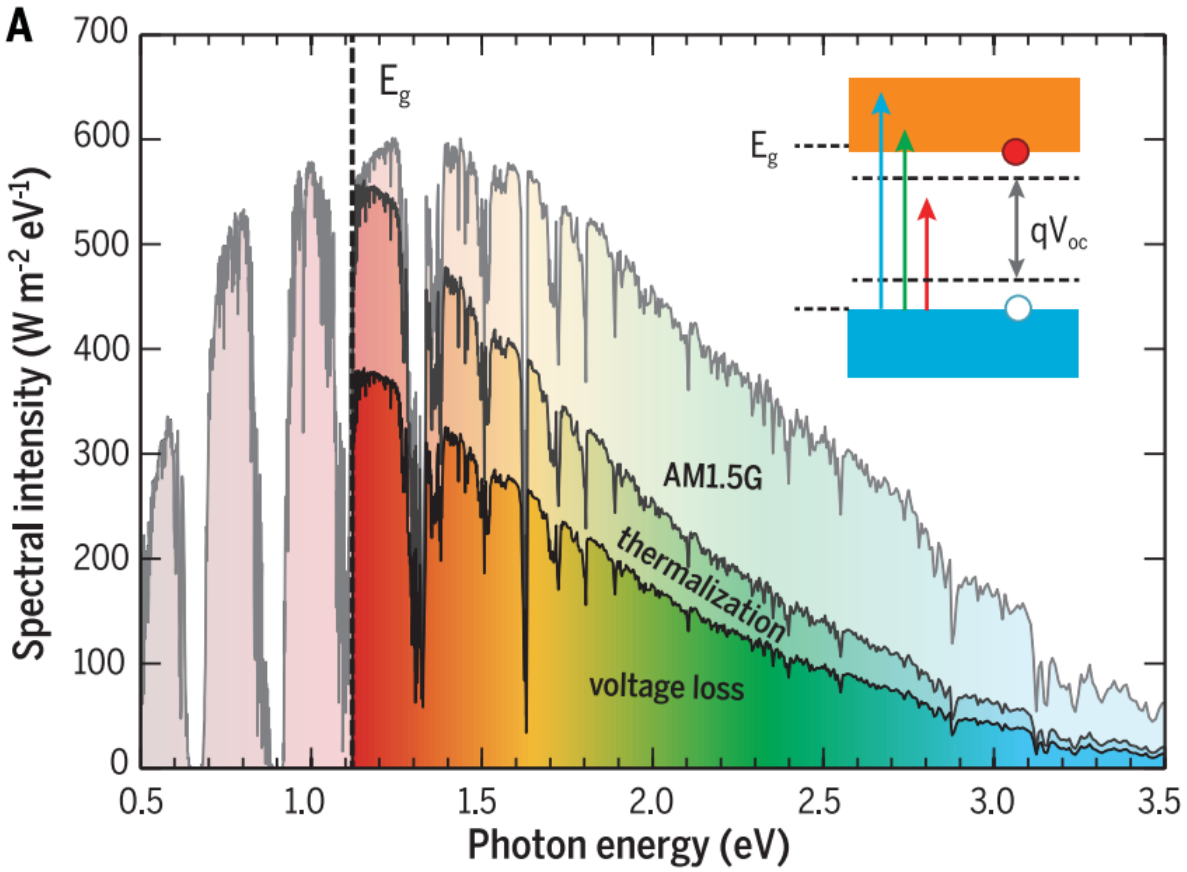

Figure 1.8: Standard solar spectrum for radiation at the top of the atmosphere. Figure taken from reference 58.

1.3 Overview of this Study

1.3.1 Promising Candidates for Solar Absorber Materials

As already discussed, to make solar energy generation on a large scale economically viable, it must be possible to make devices with an LCOE that is comparable to fossil-fuel resources, but the materials that make up the devices must also be sufficiently abundant such that there would be enough to make a substantial number of devices in the first place. For this reason there is a drive for photovoltaic materials that could be made using the lost-cost methods associated with second-generation technology, but containing only earth-abundant components. Gauging the abundance of a given material is not as trivial a process as looking at crustal abundance as supply, demand, geographical distribution and extraction must all be considered. However some conclusions can be drawn by comparing one particular material to another, for instance

the competition with the display industry for indium compared to zinc... Furthermore, another conclusion which can be drawn is that knowledge of solar cell technologies made from various different materials opens up the possibility of utilizing multiple different materials to collectively contribute to the global solar power capacity to enable larger-scale power generation from this renewable, low-carbon resource. Additionally by studying various different materials, the scientific community could eventually discover or invent some that could have the best properties to enable low-cost synthesis of highly efficient devices to eventually significantly reduce the LCOE of solar power.

Presently, two of the most studied candidate earth-abundant thin-film solar cell materials include Cu_2ZnSnS_4 (CZTS) and methylammonium lead iodide ($CH_3NH_3PbI_3$ or $MAPbI_3$) [82]. The potential of CZTS for photovoltaic applications was realised in 1988 by Ito and Nakazawa [37]. The band gap of the material has been predicted [90] and measured [65] to be 1.5 eV, which corresponds to a theoretical conversion efficiency limit of 28% as predicted by Shockley-Quiesser photon balance [67]. However, the current record device efficiency is 8.8% [73] and it is believed that this figure must be increased to at least 15% for the devices to be commercially viable [68]. PV devices composed of a CZTS absorber layer are hampered by low open circuit voltage (V_{OC}) [68], which is believed to be due to the formation of secondary phases [5] and defects [16] in CZTS, although the exact origin of the low V_{OC} remains unknown. The first component of this study is therefore an attempt to determine possible origins of this deficit in CZTS.

$MAPbI_3$ is an example of a hybrid halide perovskite solar cell material, which are regarded as a convergence of inorganic thin-film and dye-sensitised solar cells (DSSC's) [11]. Research on such materials dates back to 1928 [80]. The efficiency of $MAPbI_3$ solar cells however has increased rapidly between 2009 and 2014 from 3.8% for $MAPbI_3$-based DSSC's to 20.1% for a planar $MAPbI_3$-based thin-film solar cells [82] and has therefore surpassed the record efficiency of both conventional DSSC's as well as the earth-abundant thin-film PV absorber material CZTS [11]. The architecture of a typical photovoltaic device, such as that shown in figure (**??**), is dependent upon charge separation by variation in material composition, as in a p-n junction.

However, in ferroelectric materials charge separation can also be achieved due to the intrinsic crystal field in a homogeneous material. The crystal polarity creates microscopic electric fields across domains, separating photogenerated excitons into free charges, and segregating the transport of the free charges to reduce recombination rates [15]. Hybrid perovskites have been shown to exhibit spontaneous electric polarization [23]. Therefore, one possible explanation for the high efficiency of $MAPbI_3$-based solar cells is enhanced separation of photoexcited electron and hole pairs, and hence reduced rate of electron-hole recombination, due to the presence of ferroelectric domains [23, 11]. Although the stability of $MAPbI_3$-based solar cells has been identified as a big challenge for these devices, as $CH_3NH_3PbI_3$ is very sensitive to polar solvents such as water and so readily dissolves and decomposes into PbI_2 [55].

A number of interesting photovoltaic phenomena have been observed in ferroelectric (FE) materials such as the bulk photovoltaic effect (BPE) and the anomalous photovoltaic effect (APE) [15]. Ferroelectric materials usually have a high dielectric constant (which was mentioned earlier as an important parameter for a photovoltaic material) and they possess a spontaneous electric polarization that can be switched between two or more states using an electric field [47]. The BPE was first recorded in 1956 in $BaTiO_3$ [18], where photovoltages were measured in un-doped single crystals [15]. The BPE effect is distinctly different from the typical PV effect in semiconductor p-n junctions as it is the polarization electric field that is the driving force for the photocurrent in FE-PV devices [87]. The conventional PV effect is discussed further in section **??** and FE-PV phenomena are discussed further in section 2.8. The APE was first observed in PbS films in 1946 [71] and has since been reported in polycrystalline CdTe, ZnTe, InP [41, 26, 77], where photovoltages output along the polarization direction can be significantly larger than the band gap of the material [87], which is usually the limit for a semiconductor PV material [15]. The Shockley-Queisser limit, which prevents any single p-n junction solar cell from converting more than 33.7% of the incident light into electricity has not been predicted to apply for these photovoltaic phenomena. An upper limit for the theoretical power conversion efficiency (PCE) from this photovoltaic mechanism seems to still be an open question [54], although an ultimate maximum efficiency of any single-band gap absorber of

44% has been set by thermodynamic considerations [67]. The identification and understanding of such phenomena may open up the possibility of more efficient PV devices constructed from a number of different photoferroelectric materials. However, most of the commonly used ferroelectric materials such as $LiNbO_3$ and $BaTiO_3$ have band gaps larger than 3 eV and can therefore only absorb sunlight in the UV range to convert into electricity, which accounts for only around 3.5% of solar energy [87], which is illustrated in figure 1.8. The optimal range for the band gap in order to absorb the majority of the solar spectrum under typical radiation conditions is between 1.06 eV and 1.50 eV [36]. Research efforts have also gone into adjusting the optical absorption of ferroelectric materials without influencing the ferroelectric properties of the material through chemical doping or alloying [87]. In $Bi_4Ti_3O_{12}$ (BiT) the optical band gap has been tuned in such a way, resulting in a decrease from 3.6 eV to 2.7 eV [17], although this is still considerably larger than the optimal range for a PV absorber material.

This then leads on to the second component of this study, which is an investigation of the optoelectronic properties of new candidate solar absorber materials that may also exhibit ferroelectricity, but have band gaps within the optimal range for the absorption of sunlight. In theory, these materials may exhibit the exceptionally high performance of $MAPbI_3$-based solar cells (ideally without the instability issues suffered by $MAPbI_3$) or enable the possibility of exploiting other novel photovoltaic phenomena such as the anomalous and bulk photovoltaic effects to overcome the Shockley-Quiesser efficiency limit without the need for such complicated device architectures as in third-generation tandem solar cells. Although the difference between the Shockley-Quiesser limit and the ultimate thermodynamic limit of a solar material is not enormous, it is also possible that ferroelectric materials have properties that enable more efficient devices to be made more easily, such as good screening of the effect of defects due to a high dielectric constant or enhanced electron-hole separation from ferroelectric domains resulting in reduced recombination and a higher performance solar cell with 'low quality' defective and nanostructured materials. Such technologies could provide one possible route for the technological breakthrough that could enable economically-viable, large-scale solar energy generation.

1.3.2 Investigating Possible Bottlenecks in the Performance of CZTS (Cu_2ZnSnS_4) Devices

Mention kesterite as CZTS and CZTSe, combination of both gives highest performance but current study limited to just CZTS.

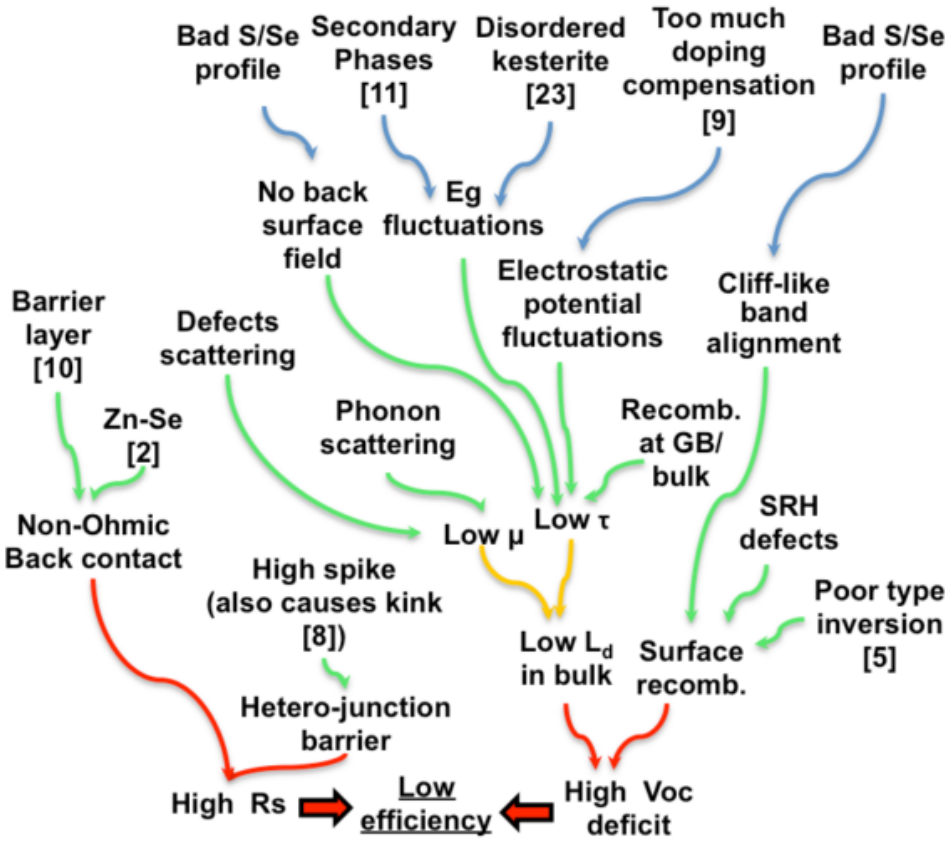

Figure 1.9: Figure take from 19.

Voc deficit + PL spectra of CZTS + disorder as a bottleneck –¿ essentially deciphering the PL spectra!

Photoluminescence (PL) spectra is discussed much more thoroughly in section 2.5, but the key point for our study is that the PL spectra of CZTS differs considerably from the ideal case (compare PL spectra of high quality Si, CdTe and CIGS?)

Although ultimately the aim is to make thin-film devices from CZTS, for the purposes of our study where we are currently simulating disorder in bulk CZTS, measurements performed on single crystals will be the most directly relatable to our findings as our model will not include

additional spectra for recombination transitions and grain boundaries.

Other disorder studies providing evidence for Cu, Zn disorder: neutron, near-resonant Raman, etc. (see old report plan)

See Kosyak paper, top of pg 2 for discussion of why defect theory is important for CZTS because of limited exptl data whilst in early stages of development.

Ultimate aim of study is to unpick/ decipher the PL spectra of CZTS to determine sources of efficiency loss to guide experiment. There are a number of possible explanations for the PL spectra such as mid gap states (which would give rise to additional sharp optical transitions and energies below the band gap of the material), band gap broadening due to intrinsic lattice vibrations but also to disorder and band tailing due to various types of disorder.

We first study band tailing from metal disorder in CZTS. We also re-investigate the formation of S vacancies when accounting for S being in the gas state, using a full S chemical potential as V_S has been predicted to give a mid gap energy state, but calculations consider S in only the solid state have predicted a high defect formation energy and therefore the presence of this type of defect unlikely. This may not be the case when accounting for S being in the gaseous state during the synthesis of CZTS. We then go on to attempt to determine how much of the band gap broadening observed in CZTS (*REF PVTEAM PAPER*) is due to disorder by calculating the intrinsic (and inevitable!) contribution from the lattice expansion of perfect CZTS at finite temperatures, and subtracting this from the experimentally measured broadening.

But there are a number of further investigations (see further work section): larger systems, domains, band gap fluc + compensating defects for off-stoichiometric systems

1.3.3 Predicting and Assessing the Properties of New Candidate Solar Absorber Materials

Ferroelectric materials in PV devices

Screening criteria

Properties of interest for PV (discussed above) which we aim to predict for these materials + known exptl and theoretical values from the literature (see MRes2 report and new bournonite paper)

Chapter 2

Background Theory

2.1 The Description of Perfect Periodic Crystal Structures

Theoretical models of crystalline solids are based around the existence of translational symmetry in a crystal lattice such that the lattice can be constructed from periodically repeating a unit cell of atoms. The Bravais lattice specifies the periodic array in which the repeated units of the crystal are arranged. A crystal lattice can therefore be described by its underlying Bravais lattice and the arrangement of atoms, ions or molecules within a particular unit cell, i.e. the basis [1]. This principle is used in a number of ways during this study. Firstly, this process is performed on a finite scale to construct a 64 atom supercell of CZTS from the 8 atom primitive unit cell for use in density functional theory (DFT) calculations. This process is discussed further in section **??** and an outline of DFT is given in section **??**. The principle is also used in the DFT calculations through the implementation of periodic boundary conditions to simulate an infinite, bulk system using only a finite supercell.

Another important concept in the theoretical modelling of periodic structures is reciprocal space and the reciprocal lattice. Converting to reciprocal space enables the description of periodic

features with a longer-range periodicity than the unit cell in real space, such as the motion of electrons in a crystal and phonons. In the same way that any quantity that varies with time can be described as a sum of Fourier components in the frequency domain; the spatial properties of a crystal can be described as a sum of components in Fourier space, otherwise known as reciprocal space or k-space. The reciprocal lattice of a perfect single crystal is an infinite periodic 3D array of points whose spacings are inversely proportional to the distances between the planes in the lattice in real space. Vectors in real space have dimensions of length, whereas vectors in reciprocal space have dimensions of length^{-1}. This can therefore be compared directly to the wavevector $\left(k = \frac{2\pi}{\lambda}\right)$ of an excitation such as a phonon or a moving electron and multiplication of each coordinate of the reciprocal lattice by $\hbar$ converts reciprocal space into momentum space as for a quantised wave $\mathbf{p} = \hbar\mathbf{k}$ [8].

The Wigner-Seitz primitive cell is the most common choice of primitive cell with the full symmetry of the Bravais lattice. It represents the region of space around a lattice point that is closer to that point than to any other lattice point. For example, figure 2.1a shows the truncated octahedron that is the Wigner-Seitz cell for a body-centred cubic (bcc) lattice [1]. The first Brillouin zone is the Wigner-Seitz primitive cell of the reciprocal lattice. The reciprocal of the bcc lattice is face-centred cubic (fcc), therefore the first Brillouin zone of of the bcc lattice is the fcc Wigner-Seitz primitive cell as shown in figure 2.1b [2]. As the full symmetry of the reciprocal lattice is contained within the first Brillouin zone, it is only necessary to sample k-points within this single unit cell of the reciprocal lattice when calculating the electronic ground state of a periodic structure.

Another important aspect of the theoretical modelling of periodic structures for this study is the motion of an electron in the periodic structure. In the band theory of solids, the energy of a single electron in a perfect crystal is described by the one-electron Schrödinger equation, shown in equation 2.3. Scattering caused by phonons or defects are introduced afterwards as a perturbation. The first term in equation 2.3 is the kinetic energy of the electron, V($\mathbf{r}$) is the effective non-zero periodic potential energy experienced by the electron in the crystal, ψ is the electron wavefunction and ϵ is the eigenenergy of the electron. In band theory, it is assumed

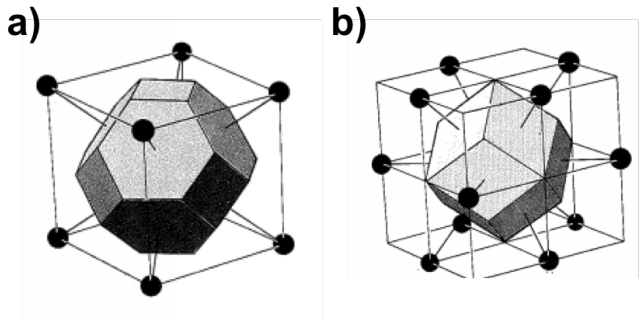

Figure 2.1: The Wigner-Seitz cell for the body-centred cubic Bravais lattice where there is a lattice point at its centre and on each vertex. The hexagonal faces bisect the lines joining the central point to the points on the vertices. The square faces bisect the lines joining the central point to the central points in each of the six neighbouring cubic cells. Figure taken from reference 1.

that for any electron everything else in the crystal can be represented by the effective potential energy, V(**r**) [9].

$$\left[\left(-\frac{\hbar^2}{2m}\right)\nabla^2 + V(\mathbf{r})\right]\psi = \epsilon\psi \tag{2.1}$$

The spatial dependence of the potential experienced by an outer electron in a crystal for multi-electron systems was considered by Felix Bloch. He determined that the total potential is the sum of two parts. Firstly, the electrostatic potential due to the array of atomic cores. For a perfect lattice this should have the translational periodicity of the lattice. Secondly, the potential due to all other electrons. Bloch assumed that the charge density would have the same long-term average value in every unit cell of the crystal and therefore would be periodic. Bloch's theorem states that the wavefunction which satisfies equation 2.3 subject to a periodic potential should be of the form shown in equation 2.4, where $U_k(\mathbf{r})$ is some function (depending on the value of the wavevector, **k**) that also has the complete periodicity of the lattice and **k** is confined to the first Brillouin zone [9].

$$\psi_k(\mathbf{r}) = U_k(\mathbf{r})e^{i\mathbf{k}\cdot\mathbf{r}} \tag{2.2}$$

Each electron occupies a state of definite **k**. Therefore, an infinite number of electrons within the solid would result in an infinite number of k-points. At each k-point, only a finite number of the available energy levels will be occupied. Therefore only a finite number of electrons need

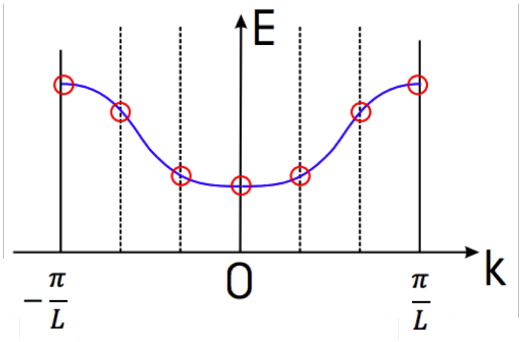

Figure 2.2: The energy dispersion relation for electrons moving in a crystal, illustrating how the function can be approximately represented by a finite number of k-points, which form an equally-spaced mesh. Figure adapted from reference 20.

to be considered but at an infinite number of k-points. In practise, all of these k-points are not considered. Electron wavefunctions will be almost identical for values of $\mathbf{k}$ that are sufficiently close, so the wavefunctions over a region of reciprocal space can be represented by considering the wavefunction at a single k-point. It is therefore sufficient to consider the electronic states at a finite number of k-points in order to determine the ground state energy of the solid. This approximation is illustrated in figure 2.2. Using Bloch's Theorem therefore has enabled the ground state energy to be determined by considering only the number of electrons in the unit cell at a finite number of k-points, which are chosen to sample the Brillouin zone appropriately. The choice here is a balance between more k-points for a more accurate representation of the Brillouin zone and fewer k-points to reduce the computational expense of the calculation [75].

2.2 Crystal Imperfections of the First and Second Types

Notes from A. Guinier 'X-Ray Diffraction': use Ch6 to introduce then Ch8 for long and short range order in mixed crystals with substitutional disorder + see Ziman + link to order parameter

2.3 Band Theory & Band Structure

See MRes2 report + use e.g. of Si, state that early figure is a simplification and use to discuss why Si is not ideal from indirect band gap, use rough calc from lecture

The band theory of solids provides a means to explain the difference in the electrical conductivity of conductors, semiconductors and insulators. Electrons bound to an atom have a number of possible discrete energy levels. When a large number of atoms are brought together to form a solid, it becomes impossible to assign individual electrons to individual atoms. Instead, the electrons are considered to be shared amongst the atomic nuclei. However, a consequence of this sharing would be a large number of electrons occupying the same energy state, which violates the Pauli Exclusion Principle. The original discrete energy levels therefore are broadened into bands. The new energy levels are so closely spaced that they are considered to be a quasi-continuous band of allowed energies. The series of bands of allowed energies in a semiconductor or insulator are separated by bands of forbidden energy, known as the band gap, E_g, of the material [88]. In the simplest model, the upper energy band (the conduction band) is separated from the lower energy band (the valence band) by a constant band gap. This is called the flat band model. In real structures, the band architecture is more complicated than this simple model[74].

The concept of the energy band model of a solid emerges from considering the behaviour of electrons in a periodic crystal lattice, but cannot be understood in terms of classical physics alone. Instead, the electron must be considered in terms of wave-mechanical terms as a wave propagating in a periodic structure with diffraction and interference effects [42]. In the band theory of solids, the energy of a single electron in a perfect crystal is described by the one-electron Schrödinger equation, shown in equation 2.3. The first term in equation 2.3 is the kinetic energy of the electron, $V(\mathbf{r})$ is the effective non-zero periodic potential energy experienced by the electron in the crystal, ψ is the electron wavefunction and ϵ is the eigenenergy of the electron. In band theory, it is assumed that for any electron, everything else in the crystal can be represented by the effective potential energy, $V(\mathbf{r})$ [9].

$$\left[\left(-\frac{\hbar^2}{2m}\right)\nabla^2 + V(\mathbf{r})\right]\psi = \epsilon\psi \tag{2.3}$$

The spatial dependence of the potential experienced by an outer electron in a crystal for multi-electron systems was considered by Felix Bloch. He determined that the total potential is the

sum of two parts. Firstly, the electrostatic potential due to the array of atomic cores. For a perfect lattice this should have the translational periodicity of the lattice. Secondly, the potential due to all other electrons. Bloch assumed that the charge density would have the same long-term average value in every unit cell of the crystal and therefore would be periodic. Bloch's theorem states that the wavefunction which satisfies equation 2.3 subject to a periodic potential should be of the form shown in equation 2.4, where $U_k(\mathbf{r})$ is some function (depending on the value of the wavevector, $\mathbf{k}$) that also has the complete periodicity of the lattice and $\mathbf{k}$ is confined to the first Brillouin zone [9].

$$\phi_k(\mathbf{r}) = U_k(\mathbf{r})e^{i\mathbf{k}\cdot\mathbf{r}} \tag{2.4}$$

$$\psi_k(\mathbf{r}) = \sum_k A_k\phi_k(\mathbf{r}) = \sum_k A_k U_k(\mathbf{r})e^{i\mathbf{k}\cdot\mathbf{r}} \tag{2.5}$$

Due to the translational symmetry of a crystal lattice, an eigenfunction of the one-electron Schrödinger equation can be expressed as a sum of Bloch functions such as that shown in equation 2.4, as shown in equation 2.5. The one-electron wavefunctions therefore can be indexed by constants $\mathbf{k}$, which are the wave vectors of the plane waves forming the 'backbone' of the Bloch function. A plot of the electron eigenenergies from equation 2.3 versus $\mathbf{k}$ is known as the electronic band structure of the crystal [86].

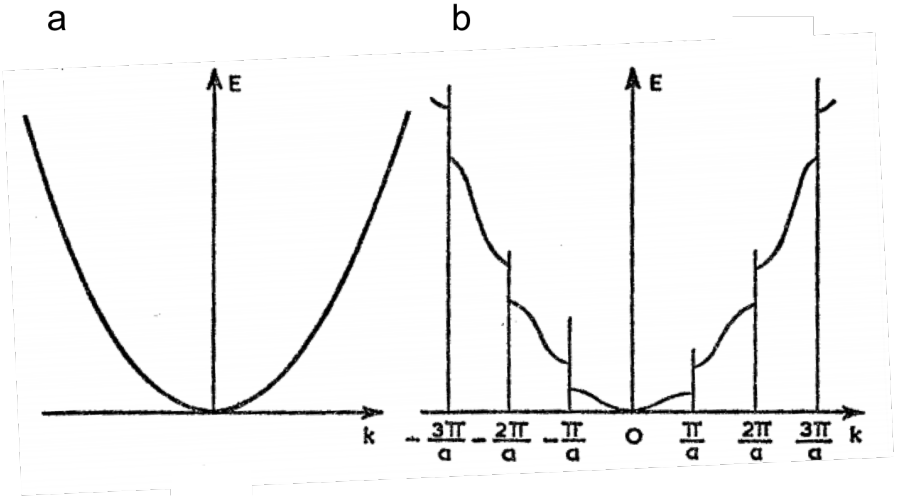

Figure 2.3: Energy-wave vector diagrams: (a) the free electron parabola, (b) modification due to a periodic crystal lattice. Figure taken from reference 42.

The introduction of a medium with a discrete structure, such as a crystal lattice, has a profound effect on the dispersion relation of the waves. The energy dispersion relation of a free electron and that in a periodic crystal lattice is shown in figure 2.3. A periodic medium does not completely suppress the propagation of waves, as would be expected in disordered or amorphous structures, but they do however introduce limiting frequencies and wavelengths for the propagation, followed by cut-off regions. The lower limit of the wavelength is set by the lattice spacing, a, giving an upper limit of the wave vector, $\mathbf{k}$, of $\frac{\pi}{a}$. As figure 2.3 shows, the parabola of the free electron in modified in a periodic crystal by the introduction of discontinuities at values of $\mathbf{k}$ corresponding to multiples of $\frac{\pi}{a}$. The appearance of such energy gaps implies that electrons in a periodic crystal may only have kinetic energies corresponding to certain bands, whilst being free to propagate in the lattice [43].

The energy band model has been successful in explaining many aspects of the behaviour of solids and a large amount of experimental data collected has supported the theoretical predictions made using the model. Its main drawback however is that is assumes a perfect, or nearly perfect, crystal lattice. It applies well to single crystals and polycrystalline substances, but cannot be applied to materials that are amorphous or heavily disordered so that the structure deviates significantly from the periodicity of the crystal [42]. Low concentrations of impurities and defects can be modelled by considering, for example, the introduction of additional donor and acceptor energy levels within the band gap of a material and the scattering of electrons and holes in the solid. However, at higher defect concentrations the band profile can be modified as shown in figure 2.4 to give rise to conductivity even at temperatures that are too low to produce excitation of carriers into the free conduction bands, called impurity band conduction [43].

A useful concept used to simplify the dynamics of an electron in a crystal lattice in the band theory of solids is that of effective mass. The effective mass is a convenient parameter which accounts for the influence of a periodic lattice on a free carrier, enabling an electron in a periodic crystal to be treated as though it were a free particle but with a different mass in calculations of charge transport. Values of effective mass in semiconductors usually vary between 0.01 and

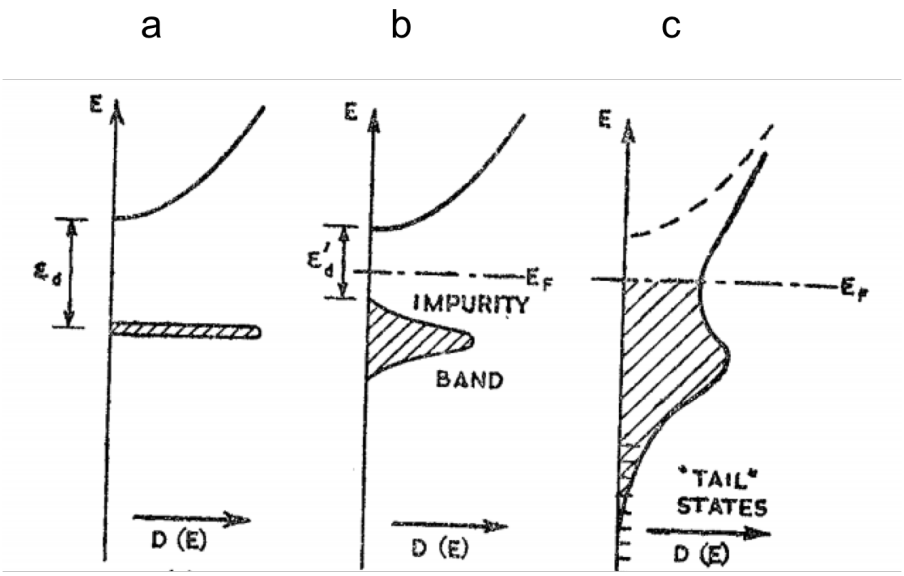

Figure 2.4: The influence of increased donor impurity density on the conduction band profile showing low (a), medium (b) and high (c) densities of impurities. Figure taken from reference 43.

1 times the mass of a free electron and it is determined by the curvature of the energy graph in **k**-vector space [43]. The effective mass is a parameter that can influence the efficiency of a solar cell, in particular, the effective mass of holes in the valence band and electrons in the conduction band (i.e. minority charge carriers) are of interest. The mobility of charge carriers is inversely proportional to the effective mass and the mobility of charge carriers in a PV material is important for efficient charge collection [4].

2.4 Spin Orbit Interaction

see webpages: pg 84 for discussion of effect of SOC on lattice without inversion symmetry! + useful slide

Look for textbook source?

2.5 Photoluminescence Spectra of Solar Absorber Materials

Photoluminescence (PL) imaging is becoming a popular method to inspect solar cell materials, it does not require a full functioning device and can be a powerful tool for probing defects in semiconductors [**?** **?**]. The PL spectra of Cu_2ZnSnS_4(CZTS) provides clear evidence of disorder in the material.

Overview of technique, information gained from technique, T dependent PL, PL spectra of CZTS: single crystal and thin film.

2.6 Band Tailing in Disordered Semiconductors

Metal disorder in CZTS due to limited cooling/ annealing times, link to Jonathan Scragg's work (years to cool to perfect crystal)

Nelson, pg 65, 3.5.4: heavy doping leading to band tailing

see Pankove + Russian 1970s papers, Urbach tail, fluctuations in electrostatic potential
See Urbach tail doc (pg 36) and use Cu/ Zn culprit paper + link to eris

+ see desktop papers from Jarv x2

2.7 Impact of Defects and Disorder on Photovoltaic Performance

SRH recomb, GBs, secondary phases, band gap and electrostatic potential fluctuations
See CMP lectures on defects + ebook reading material

2.8 Photovoltaic-Ferroelectric Phenomena & the Possibility of High Performance Solar Cells

Ferroelectric PV materials are currently receiving a great deal of research interest, however the origin of their PV properties are considered to be unresolved [84]. A large number of theories have been proposed in an attempt to explain the two observed ferroelectric-photovoltaic (FE-PV) phenomena: the bulk PV effect (BPE), also referred to as the photogalvanic effect, and the anomalous PV effect (APE). In the BPE, a direct current appears in a homogeneous medium under uniform illumination and this can occur in all materials without a center of symmetry [6]. Ferroelectric materials exhibit this effect strongly [84] and the first observation of this effect was in 1956 with photovoltages measured in un-doped single crystals of the ferroelectric material $BaTiO_3$ [18]. In the case of the APE, photovoltages have been measured that are orders of magnitude larger than the band gap of the material [71], but has been observed to disappear when the sample undergoes a phase transition to a paraelectric phase [59], and so no longer exhibits spontaneous electric polarization. Theories have been developed to explain the FE-PV phenomena based around experimental observations of factors that have been shown to influence the photovoltage of FE-PV devices, such as: the distance between the two opposite electrodes [32, 61], intensity of incident light [12], electrical conductivity [22], remnant polarization of the ferroelectric crystals [13], crystallographic orientation [31], the dimension or size of the crystals [61, 33], domain walls [83] and the interface between the FE material and the electrode [39].

Models have been proposed to explain the BPE in ferroelectric materials based upon the built-in asymmetry of non-centrosymmetric crystals. One model is based on asymmetric scattering centres in the materials [6]. In non-centrosymmetric crystals, the rate of the generation of charge carriers with momenta $\pm$k can be different due to asymmetric electron-hole scattering. A 'ballistic current' can then be generated due to the momentum imbalance [44]. Another model, the shift current model [44], has been proposed, which is based on the asymmetry of the electron density [15]. Light-induced transitions of charge carriers between bands in reciprocal

space are accompanied by asymmetrical shifts in real space between atoms in elementary cells [44]. Such currents have been demonstrated for a number of materials, such as GaAs [69] and $BiFeO_3$, where this has been demonstrated using both computational [85] and experimental [40] techniques. The shift current model has been used in first principles calculations to reproduce experimental photocurrent direction and magnitude as a function of light frequency resulting from the BPE in $BaTiO_3$[84]. The nonlinear dielectric model has also been proposed to explain the BFE effect in (Pb, La)(Zr, Ti)O_3 (PLZT) ceramics [59]. This material exhibits the photostrictive effect, where strain is induced in the sample by incident light. In this model, the large photovoltage is believed to be due to the nonlinear response of the material to the incident light, which results in an effective DC electric field throughout the ferroelectric material [87].

The domain wall theory has been proposed to explain the large generated photovoltages in the APE [7] and the Schottky-junction effect [89] and depolarization field model [14, 72], also referred to as the screening effect, have been proposed as additional contributions to the large photovoltage. Unlike the BPE, some theories to explain the APE rely on the nano- and microstructure of the material [15]. The latter two theories are related to the interface between the FE material and an electrode in a FE-PV device, but were originally neglected as the contributions to the photovoltage were believed to be small. However, these effects become more significant in thin-film devices where photovoltages are typically low [87], and thin-films are particularly relevant for PV applications. The domain wall theory was developed to explain observations of photovoltages in thin films of $BiFeO_3$ increasing linearly with the total number of ferroelectric domain walls along the net direction of electric polarization and vanishing along the direction perpendicular to the net polarization [83]. In this theory, the narrow ferroelectric domain walls drive the dissociation of photogenerated excitons and so act as nanoscale photovoltage generators connected in series. The photocurrent across the domain walls is therefore continuous but the photogenerated voltage accumulates along the direction of net polarization, allowing for photovoltages that are considerably larger than the band gap of the material [87]. In the Schottky-junction effect, the FE semiconductor forms a Schottky contact with the metal electrodes, which then generate a photocurrent under illumination due to the local electric field

caused by the band bending near to the electrode. This photocurrent is dependent upon the Schottky barrier height and depletion region depth, but the photovoltage is still limited to the band gap of the material. Further, the additional photovoltage contribution from this effect can be cancelled out if the same electrode contacts are used, due to the opposite polarization of the two Schottky-junctions [87]. In the depolarization field model, high densities of polarization charges are believed to accumulate on surfaces of polarized FE films, this then induces a large electric field inside the FE layer if the charge is not screened. This effect will be far more pronounced in a thin-film device. The electric field is thought to not be fully screened by the free charges in the metal or semiconductor that the FE layer is in contact with, resulting in a depolarization field. This depolarization field will be larger when the FE material has a large remnant electric polarization, the FE layer is thinner and when it is in contact with a semiconductor, as opposed to a metal, due to fewer free charge carriers and higher dielectric constant in a semiconductor than a metal, giving weaker screening. The depolarization field is believed to be the dominating force for the separation of photogenerated charge carrier pairs [87].

Chapter 3

Methodology

3.1 Calculation of the Formation Energies of Defects in Cu_2ZnSnS_4

3.1.1 Density Functional Theory & Hybrid Functionals

Go through different levels of theory used in calculations done at Duke with emphasis on hybrids for the defect calcs and why?

3.1.2 The Supercell Method & Charged Defects

Discuss convergence of edge geometry? + see Aron's lectures

3.1.3 Quasichemical Theory for Point Defects

See Kosyak paper, ref 19. + second page for discussion of non-interacting defects in quasichemical formalism + notes from Aron's defect sessions

3.1.4 Chemical Potential and Defect Formation Energy as a Function of Temperature and Pressure for V_S

3.2 Monte Carlo Simulation of On-Lattice Disorder in Cu_2ZnSnS_4

- General MC simulations and Metropolis algorithm
- Ising model and likeness of our simulation to ising model
- Convergence problem - difference in electrostatics summation compared to spin summation in standard ising model, briefly Ewald summation (implemented in GULP) but too comp intensive for our simulations, convergence w.r.t r, approx using some region for summation before and after swap, comparison to gulp full Ewald summation for final config (but far too comp expensive to use for each 1000's of step of MCS in simulation!)
- See GULP manual Methods section (pg 11) - eris stops at pairwise interactions whereas gulp goes to higher order terms + parameterises for higher order terms to compensate?

3.2.1 Multi-Scale Monte Carlo Simulations of Thermodynamic Disorder

DFT scaling: correcting bulk/ macroscopic dielectric constant with DFT to account for dielectric screening (HSE vs gulp plot)

3.2.2 Convergence Tests for the Model

- convergence of dE in MCS wrt gulp
- conv in dist of accepted moves to boltzmann

- check against known end points: reproducing kesterite ground state + infinite T fully disordered limit

3.2.3 Calculation of Order Parameters

Long range - RDF Short range - local environment of Sn?

3.2.4 Determination of Band Tailing from Monte Carlo Simulations

3.3 Calculation of Intrinsic Band Gap Broadening in Cu_2ZnSnS_4

3.4 Calculation of Optoelectronic Properties of Sulfosalt Materials

Chapter 4

Results

4.1 Investigation of Performance Bottlenecks in Cu_2ZnSnS_4

4.1.1 Project1: Band Tailing due to Substitutional Disorder Amongst Cations

4.1.2 Project2: Re-Assessing the Formation Energy of V_S

4.1.3 Project3: Intrinsic Band Gap Broadening from Lattice Vibrations

4.2 Prediction and Assessment of Optoelectronic Properties of Sulfosalt Materials for Photovoltaic Applications

Re-introduce materials briefly

4.2.1 Band Structures & Band Gap

4.2.2 Effective Masses

4.2.3 Dielectric Functions

4.2.4 Absorption Coefficients

Chapter 5

Conclusion

5.1 Project 1

5.2 Project 2

5.3 Project 3

5.4 Future Work

Future Work.

- GBs in CZTS: Comparison to David's HRTEM images? Keith's code for lattice strain/ plausibility of interfaces, workfunction calculations
- methodology development with eris - algorithm development to simulate larger systems (e.g. parallelization by domain decomposition)
- Simulations to determine most likely surface terminations to inform exptl strategies for surface passivation?

Bibliography

[1] N. Ashcroft and N. Mermin. *Crystal Lattices*. Saunders College Publishing, 1976.

[2] N. Ashcroft and N. Mermin. *The Reciprocal Lattice*. Saunders College Publishing, 1976.

[3] E. P. I. Association. Global market outlook for photovoltaics 2014-2018. 2014.

[4] M. Balkanski and R. F. Wallis. *Introduction to Transport in Semiconductors*. OUP Oxford, 2000.

[5] W. Bao and M. Ichimura. Influence of Secondary Phases in Kesterite-Cu 2 ZnSnS 4 Absorber Material Based on the First Principles Calculation. *Int. J. Photoenergy*, 2014(c), 2014.

[6] V. Belinicher and B. Sturman. The photogalvanic effect in media lacking a center of symmetry. *Uspekhi Fiz. Nauk*, 130(3):415, 1980.

[7] A. Bhatnagar, A. Roy Chaudhuri, Y. Heon Kim, D. Hesse, and M. Alexe. Role of domain walls in the abnormal photovoltaic effect in BiFeO. *Nat. Commun.*, 4(May):2835, 2013.

[8] J. Blakemore. *Crystallinity and the Form of Solids: Reciprocal Space*. Cambridge University Press, 1985.

[9] J. Blakemore. *Electrons in Metals: The band Theory of Solids*. Cambridge University Press, 1985.

[10] M. Bokalič and M. Topič. *Spatially Resolved Characterization in Thin-Film Photovoltaics*.

[11] F. Brivio, A. B. Walker, and A. Walsh. Structural and electronic properties of hybrid perovskites for high-efficiency thin-film photovoltaics from first-principles. *APL Mater.*, 1(4):042111, 2013.

[12] P. Brody. Large polarization-dependent photovoltages in ceramic batio3 + 5 wt.catio3. *Solid State Communications*, 12(7):673 – 676, 1973.

[13] P. S. Brody. Semiconductor-ferroelectric nonvolatile memory using anomalous high photovoltages in ferroelectric ceramics. *Applied Physics Letters*, 38:153–155, Feb. 1981.

[14] P. S. Brody and B. J. Rod. Decay of remanent polarization in ferroelectric films using polarization-dependent photovoltages. *Integrated Ferroelectrics*, 3(3):245–257, 1993.

[15] K. T. Butler, J. M. Frost, and A. Walsh. Ferroelectric Materials for Solar Energy Conversion: Photoferroics Revisited. (December):1–11, 2014.

[16] S. Chen, X. G. Gong, A. Walsh, and S.-H. Wei. Defect physics of the kesterite thin-film solar cell absorber Cu[sub 2]ZnSnS[sub 4]. *Appl. Phys. Lett.*, 96(2):021902, 2010.

[17] W. S. Choi, M. F. Chisholm, D. J. Singh, T. Choi, G. E. Jellison, and H. N. t. . Lee.

[18] A. G. Chynoweth. Surface space-charge layers in barium titanate. *Phys. Rev.*, 102:705–714, May 1956.

[19] E. S. Cortezon, R. Aninat, and E. Sanchez-cortezon. Kesterite-based photovoltaic devices: Challenges for scale-up. In *Proceedings of the IEEE Photovoltaic Specialist*, 2016.

[20] A. Eichler. *Sampling the Brillouin Zone*, 2014 (Accessed on April 28, 2015).

[21] F. I. for Solar Energy Systems ISE. *Levelized Cost of Electricity Renewable Energy Technologies*, 2013 (Accessed on Aug 3, 2015).

[22] V. Fridkin. *Photo-ferroelectrics*. Springer-Verlag Berlin Heidelberg, 1979.

[23] J. M. Frost, K. T. Butler, F. Brivio, C. H. Hendon, M. van Schilfgaarde, and A. Walsh. Atomistic origins of high-performance in hybrid halide perovskite solar cells. *Nano Lett.*, 14(5):2584–90, May 2014.

[24] C. D. Ginley, David S. Cambridge University Press, 2012.

[25] J. E. Girard. *Principles of Environmental Chemistry.* Jones & Bartlett Learning, LLC, 2014.

[26] B. Goldstein and L. Pensak. *J. Appl. Phys.*, 155, 1959.

[27] M. Grätzel. Solar energy conversion by dye-sensitized photovoltaic cells. *Inorganic Chemistry*, 44(20):6841–6851, 2005. PMID: 16180840.

[28] J. L. Gray. *The Physics of the Solar Cell*, pages 61–112. John Wiley & Sons, Ltd, 2005.

[29] W. Hermes, D. Waldmann, M. Agari, K. Schierle-Arndt, and P. Erk. Emerging Thin-Film Photovoltaic Technologies. *Chemie Ingenieur Technik*, 87(4):376–389, 2015.

[30] C. Honsberg and S. Bowden. *Open-Circuit Voltage*, 2014 (Accessed on April 28, 2015).

[31] M. Ichiki, H. Furue, T. Kobayashi, R. Maeda, Y. Morikawa, T. Nakada, and K. Nonaka. *Appl. Phys. Lett.*, 87:222903, 2005.

[32] M. Ichiki, R. Maeda, Y. Morikawa, Y. Mabune, T. Nakada, and K. Nonaka. *Appl. Phys. Lett.*, 84:395–397, 2004.

[33] M. Ichiki, Y. Morikawa, Y. Mabune, and T. Nakada. *J. Eur. Ceram. Soc.*, 24:1709–1714, 2004.

[34] F. S. Inc. *Emissions from Photovoltaic Life Cycles*, 2009 (Accessed on April 18, 2015).

[35] S. J. C. Irvine. RSC Energy and Environment Series, 2014.

[36] K. Ito. *An Overview of CZTS-Based Thin-Film Solar Cells.* John Wiley & Sons, 2015.

[37] K. Ito and T. Nakazawa. *Jpn. J. Appl. Phys.*, 27:2094–2097, 1998.

[38] J. Jean, P. R. Brown, R. L. Jaffe, T. Buonassisi, and V. Bulovic. Pathways for Solar Photovoltaics. *Energy Environ. Sci.*, 2015.

[39] W. Ji, K. Yao, and Y. C. Liang. *Adv. Mater.*, 22:1763–1766, 2010.

[40] W. Ji, K. Yao, and Y. C. Liang. Bulk photovoltaic effect at visible wavelength in epitaxial ferroelectric bifeo3 thin films. *Advanced Materials*, 22(15):1763–1766, 2010.

[41] H. R. Johnson, R. H. Williams, and C. H. B. Mee. The anomalous photovoltaic effect in cadmium telluride. *Journal of Physics D: Applied Physics*, 8(13):1530, 1975.

[42] A. K. Jonscher. *The Electronic Structure of Solids*. Routledge & Kegan Paul Ltd., 1965.

[43] A. K. Jonscher. *The Imperfect Solid*. Routledge & Kegan Paul Ltd., 1965.

[44] P. Kral. Quantum kinetic theory of shift-current electron pumping in semiconductors. *Journal of Physics: Condensed Matter*, 12(22):4851, 2000.

[45] D. W. Lane, K. J. Hutchings, R. McCracken, and I. Forbes. *New Chalcogenide Materials for Thin Film Solar Cells*. The Royal Society of Chemistry, 2015.

[46] M. Lang and A. Lang. *Overview Renewable Energy Sources Act*, 2014 (Accessed on 05 May, 2016).

[47] M. E. Lines and A. M. Glass. Oxford University Press, 1977.

[48] D. Ltd. *What is Levelised Cost of Energy (LCOE)?*, 2011 (Accessed on Aug 10, 2015).

[49] A. McEvoy, T. Markvart, and L. C. ner. *Practical Handbook of Photovoltaics - Fundamentals and Applications*. Elsevier, 2012.

[50] J. Nelson. *Introduction*. Imperial College Press, 2003.

[51] U. D. of Energy. Energy efficiency and renewable energy: 2008 solar technologies market report. 2010.

[52] U. of Oregon Investment Group. *First Solar, Inc*, 2011 (Accessed on 05 May, 2016).

[53] M. I. of Technology. *The Future of Solar Energy*, 2015 (Accessed on June 9, 2015).

[54] C. Paillard, X. Bai, I. C. Infante, M. Guennou, G. Geneste, M. Alexe, J. Kreisel, and B. Dkhil. Photovoltaics with Ferroelectrics: Current Status and Beyond. *Adv. Mater.*, apr 2016.

[55] G. Peng, X. Xu, and G. Xu. Hybrid organic-inorganic perovskites open a new era for low-cost, high efficiency solar cells. *Journal of Nanomaterials*, 2014.

[56] C. Persson and A. Zunger. Anomalous grain boundary physics in polycrystalline cuinse$_2$: The existence of a hole barrier. *Phys. Rev. Lett.*, 91:266401, Dec 2003.

[57] C. Persson and A. Zunger. Compositionally induced valence-band offset at the grain boundary of polycrystalline chalcopyrites creates a hole barrier. *Appl. Phys. Lett.*, 87(21):211904, 2005.

[58] A. Polman, M. Knight, E. C. Garnett, B. Ehrler, and W. C. Sinke. Photovoltaic materials: Present efficiencies and future challenges. *Science*, 352(6283), 2016.

[59] P. Poosanaas, K. Tonooka, and K. Uchino. Photostrictive actuators. *Mechatronics*, 10(45):467 – 487, 2000.

[60] I. E. A. P. P. S. Programme. Trends in photovoltaic applications, 19th edition. 2014.

[61] M. Qin, Y. C. Yao, Kand Liang, and S. Shannigrahi. *J. Appl. Phys.*, 101:014104–014108, 2007.

[62] K. Ramanathan and et al. *Prog. Photovolt. Res. Appl.*, 2003.

[63] T. Saga. Advances in crystalline silicon solar cell technology for industrial mass production. *NPG Asia Mater.*, 2(3):96–102, 2010.

[64] H. W. Schock. *Adv. Solid State Phys.*, page 147, 1994.

[65] J.-S. Seol, S.-Y. Lee, J.-C. Lee, H.-D. Nam, and K.-H. Kim. Electrical and optical properties of cu2znsns4 thin films prepared by rf magnetron sputtering process. *Solar Energy Materials and Solar Cells*, 75(12):155 – 162, 2003. {PVSEC} 12 Part {II}.

[66] A. Shah, P. Torres, R. Tscharner, N. Wyrsch, and H. Keppner. Photovoltaic technology: The case for thin-film solar cells. *Science*, 285(5428):692–698, 1999.

[67] W. Shockley and H. J. Queisser. Detailed balance limit of efficiency of pn junction solar cells. *Journal of Applied Physics*, 32(3), 1961.

[68] S. Siebentritt and S. Schorr. Kesterites-a challenging material for solar cells. *Prog. Photovoltaics Res. Appl.*, 20(February):512–519, 2012.

[69] J. E. Sipe and A. I. Shkrebtii. Second-order optical response in semiconductors. *Phys. Rev. B*, 61:5337–5352, Feb 2000.

[70] T. G. E. Society. *Introduction and the history of photovoltaics*. Routledge, 2013.

[71] J. Starkiewicz, L. Sosnowski, and O. Simpson. *Nature*, 158, 1946.

[72] S. Sun and P. A. Fuierer. Modeling of depolarization in ferroelectric thin films. *Integrated Ferroelectrics*, 23(1-4):45–64, 1999.

[73] S. Tajima, T. Itoh, H. Hazama, K. Ohishi, and R. Asahi. Improvement of the open-circuit voltage of cu 2 znsns 4 solar cells using a two-layer structure. *Applied Physics Express*, 8(8):082302, 2015.

[74] R. J. D. Tilley. *Colour in Metals, Semiconductors and Insulators*. John Wiley & Sons, Ltd, 2011.

[75] P. R. Tulip. Dielectric and Lattice Dynamical Properties of Molecular Crystals via Density Functional Perturbation Theory: Implementation within a First Principles Code, 2004.

[76] T. Urban. *The Deal With Solar*, 2016 (Accessed on 23 April, 2016).

[77] M. D. Uspenskii, N. G. Ivanova, and M. I. E. *Sov. Phys.- Semicond*, page 1059, 1968.

[78] J. Vidal. *UK and Germany break solar power records*, 2014 (Accessed on 04 May, 2016).

[79] H. Wirth. *Recent Facts about Photovoltaics in Germany*, 2015 (Accessed on 04 May, 2016).

[80] R. W. Wyckoff. *Am. J. Sci*, pages 349–359, 1928.

[81] J. Yan and B. R. Saunders. Third-generation solar cells: a review and comparison of polymer:fullerene, hybrid polymer and perovskite solar cells. *RSC Adv.*, 4:43286–43314, 2014.

[82] Y. Yan, W.-J. Yin, T. Shi, F. Hong, J. Ge, Y. Yue, W. Ke, D. Zhao, and A. Cimaroli. Theoretical and experimental study of earth-abundant solar cell materials. In *Active-Matrix Flatpanel Displays and Devices (AM-FPD), 2015 22nd International Workshop on*, pages 57–60, July 2015.

[83] S. Y. Yang, J. Seidel, S. J. Byrnes, P. Shafer, C. H. Yang, M. D. Rossell, P. Yu, Y. H. Chu, J. F. Scott, and J. W. Ager. *Nat. Nanotechnol.*, 5:143–147, 2010.

[84] S. M. Young and A. M. Rappe. First principles calculation of the shift current photovoltaic effect in ferroelectrics. *Phys. Rev. Lett.*, 109(11):1–5, 2012.

[85] S. M. Young, F. Zheng, and A. M. Rappe. First-principles calculation of the bulk photovoltaic effect in bismuth ferrite. *Phys. Rev. Lett.*, 109:236601, Dec 2012.

[86] P. Y. Yu and M. Cardona. *Electronic Band Structures*. Springer-Verlag Berlin Heidelberg, 2010.

[87] Y. Yuan, Z. Xiao, B. Yang, and J. Huang. Arising applications of ferroelectric materials in photovoltaic devices. *J. Mater. Chem. A*, 2(17):6027, 2014.

[88] A. A. Zaky and R. Hawley. *Dielectric Solids*. Routledge & Kegan Paul, Ltd, 1970.

[89] J. Zhang, X. Su, M. Shen, Z. Dai, L. Zhang, X. He, W. Cheng, M. Cao, and G. Zou. Enlarging photovoltaic effect: combination of classic photoelectric and ferroelectric photovoltaic effects. *Scientific Reports*, 3:2109, 2013.

[90] H. Zhao and C. Persson. Optical properties of cu(in,ga)se2 and cu2znsn(s,se)4. *Thin Solid Films*, 519(21):7508 – 7512, 2011. Proceedings of the {EMRS} 2010 Spring Meeting Symposium M: Thin Film Chalcogenide Photovoltaic Materials.